JOURNAL OF APPLIED ELECTROCHEMISTRY 21 (1991) 409–414

Dynamic simulation of the charge–discharge characteristics of the sodium–sulphur cell

H. KAWAMOTO

Advanced Reactor and Nuclear Fuel Cycle Department, Hitachi Works, Hitachi, Ltd., 3-chome, 1-1, Saiwai-cho, Hitachi-shi, Ibaraki-ken 317, Japan

Received 6 July 1990; 27 September 1990

A dynamic model of the porous sulphur electrode including diffusion of the reactant is developed to simulate charge–discharge characteristics of the sodium–sulphur cell and transient behaviour of the cell after termination of operation. From the results of investigations the following are clarified: (1) sodium ion concentration on the solid electrolyte side is low during charge, on the other hand, it is high during discharge; (2) an insulating film of sulphur is formed at the surface of the solid electrolyte in the deeply charged stage. This results in an increase of the cell resistance and thus restricts charge acceptance; (3) the resistance in the single phase region is larger than that in the two phase region; and (4) open circuit voltage in the single phase region, observed after termination of operation, is not equal to the equilibrium value but gradually approaches it according to the concentration relaxation. These characteristics agree well with experimental results.

Nomenclature

a_s	effective surface area per unit volume of the graphite matrix ($cm^2\,cm^{-3}$)
c	molar concentration ($mol\,cm^{-3}$)
D	diffusion coefficient of electrolyte, Na_2S ($cm^2\,s^{-1}$)
$D_{+,-}$	diffusion coefficient of sodium ion and sulphur ion ($cm^2\,s^{-1}$)
F	Faraday constant (96 487 C)
I	total current (A)
$\mathbf{J}$	current density ($A\,cm^{-2}$)
j_{ex}	exchange current density ($A\,cm^{-2}$)
K_p	surface polarization resistance coefficient ($\Omega\,cm^2$)
L	longitudinal length of sulphur electrode (cm)
OCV(t)	quasi-open circuit voltage observed after termination of operation (V)
p	porosity of sodium polysulphide melt
R	resistance of the cell (Ω)
R_0	resistance of the solid electrolyte, the sodium electrode and electronic components (Ω)
r	radial coordinate (cm)
r_i	inner (solid electrolyte side) radius of sulphur electrode (cm)
r_o	outer (metal container side) radius of sulphur electrode (cm)
t	time (s)
t_+	transference number of sodium ion
V	volume of sulphur electrode, $\pi(r_o^2 - r_i^2)L$ (cm^3)
W_s	weight of initially charged sulphur (g)
x	molar fraction of sulphur in sodium polysulphide (x in Na_2S_x)
z	charge number
μ	local potential (V)
$\bar{\mu}$	equilibrium potential (V)
σ	electric conductivity ($S\,cm^{-1}$)
ϕ	electric potential (V)
ϕ_0	electronic potential at outer radius of sulphur electrode (V)

Subscripts

e	electronic conduction
i	ionic conduction
+	sodium ion, Na^+
−	sulphur ion, S^{2-}

1. Introduction

The porous sulphur electrode, which is composed of sulphur and/or sodium polysulphide melt and graphite matrix, is one of the most important components which determines the sulphur utilization and the energy efficiency of the sodium–sulphur cell [1]. For this reason, many mathematical models for the sulphur electrode have been developed, as summarized [2], in attempts to understand how the performance of the cell is affected by parameters of the sulphur electrode and operating conditions. These models were successful in simulating the electrode performance in the single phase region (Na_2S_x, $x < 5.24$) and to clarify the qualitative mechanism of polarization in the two phase region (S, Na_2S_5). However, since any previous model has neglected the effect of diffusion of the reactant, quantitative evaluation of the electrode performance has been insufficient in the two phase region.

The purpose of the present work is to establish a time-dependent model which is able to simulate the

0021-891X/91 $03.00 + .12 © 1991 Chapman and Hall Ltd.

dynamic behaviour of the electrode, not only over the complete range of operation, but also after termination of operation by taking in diffusion of the reactant.

2. Modeling

2.1. *Fundamental equations*

Ionic flux in the sodium polysulphide melt and relationships between transport properties of the melt are [3]

$$\mathbf{J}_i = -\sigma_i \nabla\phi_i - F(z_+ D_+ \nabla c_+ + z_- D_- \nabla c_-), \quad (1)$$

$$D = \frac{D_+ D_- (z_+ - z_-)}{z_+ D_+ - z_- D_-}, \quad (2)$$

$$t_+ = \frac{z_+ D_+}{z_+ D_+ - z_- D_-}, \quad (3)$$

where $\mathbf{J}$ is the current density; σ is the electric conductivity; ϕ is the electric potential; F is the Faraday constant; z is the charge number of the ionic species; D is the diffusion coefficient; c is the molar concentration; t_+ is the transference number of the sodium ion. The subscript 'i' refers to the ionic conduction, and the subscripts '+' and '−' refer to the sodium ion Na^+, and the sulphur ion S^{2-}, respectively. Since $z_+ = 1$, $z_- = -2$, and $c_+ = 2c_-$ in the present system, substitution of Equation 2 and 3 into Equation 1 gives

$$\mathbf{J}_i = -\sigma_i \nabla\phi_i - \tfrac{1}{3} FD \frac{3t_+ - 1}{t_+(1 - t_+)} \nabla c_+ \quad (4)$$

Equation 4 means that the ionic current in the sulphur electrode is induced by migration and diffusion due to the gradient of the sodium ion concentration.

On the other hand, the electronic current in the graphite matrix phase is induced only by the gradient of the electronic potential, i.e. the electronic conduction is expressed as Ohm's law.

$$\mathbf{J}_e = -\sigma_e \nabla\phi_e, \quad (5)$$

where the subscript 'e' refers to electronic conduction.

Since the transference number of the sodium ion is almost unity [8], the time differential of the sodium ion concentration is equal to the divergence of the ionic current density.

$$\frac{\partial c_+}{\partial t} = -\frac{1}{F} \nabla \cdot \mathbf{J}_i \quad (6)$$

Here, the effect of convection is neglected, because the reactant is sustained in the graphite matrix [2].

From the current conservation, the divergence of the total current density is equal to zero.

$$\nabla \cdot (\mathbf{J}_i + \mathbf{J}_e) = 0. \quad (7)$$

Since the exchange current density at the surface of graphite is small compared with the limiting current density (i.e. the exchange current density is of the order of several $mA\,cm^{-2}$ (see Fig. 4), whereas the limiting current density is $28–100\,mA\,cm^{-2}$ [4]), the exchange current density is assumed to be proportional to the reaction overpotential [2, 9, 12, 13]. Under this assumption, the following linear relationships are determined in the porous sulphur electrode where ionic and electronic conduction coexist.

$$\phi_e - \phi_i - \mu = K_p j_{ex}, \quad (8)$$

$$\nabla \cdot \mathbf{J}_i = -\nabla \cdot \mathbf{J}_e = a_s j_{ex}, \quad (9)$$

where μ is the local potential, K_p is the surface polarization coefficient, j_{ex} is the exchange current density, and a_s denotes the effective surface area per unit volume of the graphite matrix. By substituting Equations 4, 5 and 8 into Equation 9, the following coupled linear differential equations are obtained.

$$-\nabla \cdot (\sigma_i \nabla\phi_i) + \frac{a_s}{K_p}\phi_i = \tfrac{1}{3} F \nabla \cdot \left\{ D \frac{3t_+ - 1}{t_+(1 - t_+)} \nabla c_+ \right\} + \frac{a_s}{K_p}(\phi_e - \mu), \quad (10)$$

$$-\nabla \cdot (\sigma_e \nabla\phi_e) + \frac{a_s}{K_p}\phi_e = \frac{a_s}{K_p}(\phi_i + \mu). \quad (11)$$

Substituting Equations 8 and 9 into Equation 6, modifies Equation 6 as

$$\frac{\partial c_+}{\partial t} = \frac{a_s}{K_p}(\phi_e - \phi_i - \mu). \quad (12)$$

Equations 10, 11, and 12 are basic to deriving the time-dependent distributions of the ionic potential, the electronic potential, and the sodium ion concentration in the electrode.

2.2. *One-dimensional expressions*

Since sodium–sulphur cells are usually designed in tubular form, the one-dimensional cylindrical coordinate system is employed to perform numerical calculations. The one-dimensional expressions of equations 10 and 11 in cylindrical coordinates are

$$-\frac{\partial}{\partial r}\left(r\sigma_i \frac{\partial\phi_i}{\partial r}\right) + r\frac{a_s}{K_p}\phi_i = \tfrac{1}{3} F \frac{\partial}{\partial r} \times \left\{ rD \frac{3t_+ - 1}{t_+(1 - t_+)} \frac{\partial c_+}{\partial r} \right\} + r\frac{a_s}{K_p}(\phi_e - \mu) \quad (13)$$

$$-\frac{\partial}{\partial r}\left(r\sigma_e \frac{\partial\phi_e}{\partial r}\right) + r\frac{a_s}{K_p}\phi_e = r\frac{a_s}{K_p}(\phi_i + \mu) \quad (14)$$

Since the ionic current is insulated at the surface of the metal container, on the other hand, the electronic current is insulated at the surface of the solid electrolyte, boundary conditions corresponding to the present system during charge discharge operations are

$$\phi_i = 0, \quad \partial\phi_e/\partial r = 0 \quad \text{at} \quad r = r_i,$$
$$\partial\phi_i/\partial r = 0, \quad \phi_e = \phi_0 \quad \text{at} \quad r = r_o \quad (15)$$

where r_i is the inner radius of the electrode and r_0 is the outer radius of the electrode. The fixed boundary condition, ϕ_0, is determined implicitly so as to satisfy the following integral equation.

$$I = \int_V a_s j_{ex}\, dV = -2\pi L \int_{r_i}^{r_o} \frac{a_s}{K_p}(\phi_e - \phi_i - \mu) r\, dr, \quad (16)$$

where I is the total current flowing through the cell, L is the longitudinal length of the electrode, and V denotes the volume of the sulphur electrode. Equations 12, 13 and 14 are solved numerically by the one-dimensional iterative finite element method from the initial condition

$$c_+(r, t = 0) = c_{+0}(r, t = 0), \quad (17)$$

under boundary conditions in Equation 15 so as to satisfy Equation 16. The resistance of the cell, R, can be calculated by the following equation

$$R = [(\bar{\mu} - \phi_0)/I] + R_0 \quad (18)$$

where $\bar{\mu}$ denotes equilibrium potential determined from the averaged molar fraction of sulphur [5], and R_0 includes the resistance of the solid electrolyte, the sodium electrode and electronic components.

Since no current flows into or out of the boundaries when operations are terminated, the boundary conditions after termination of operation are

$$\partial\phi_i/\partial r = 0 \quad \text{at} \quad r = r_i, r_o$$
$$\partial\phi_e/\partial r = 0 \quad \text{at} \quad r = r_i, r_o \quad (19)$$

instead of Equation 15, and the distribution of the sodium ion concentration calculated just before termination of operation is adopted for the initial condition. The quasi-open circuit voltage observed after termination of operations, OCV(t), can be calculated by the following equation.

$$\text{OCV(t)} = \phi_e(r = r_o) - \phi_i(r = r_i). \quad (20)$$

2.3. *Determination and simplification of constants*

The effective conductivity of the sodium polysulphide melt and the effective surface area of the graphite matrix in contact with the melt are assumed to be linearly related to the volumetric density of sodium polysulphide [2, 12].

$$\sigma_i = \sigma_{i0}(1 - p),$$
$$a_s = a_{s0}(1 - p)\begin{cases} \times \quad 1 & x < 5.24 \\ \times \ (5.24/x) & x > 5.24 \end{cases} \quad (21)$$

where p is the porosity of the melt, and σ_{i0} and a_{s0} are the net values of the ionic conductivity of the melt and the surface area per unit volume of the graphite matrix, respectively. The molar fraction of sulphur, x in Na_2S_x, is associated with the sodium ion concentration.

$$x = \left(\frac{2}{c_+}\right)\left(\frac{W_s}{32}\right)\left(\frac{1}{V}\right) \quad (22)$$

where W_s is weight of initially charged sulphur. The transport parameters, σ_{i0}, D, t_+, and μ are reported in [5–8] respectively.

3. Results and discussion

3.1. *Charge–discharge characteristics*

Figures 1–3 show the calculated and measured charge–discharge characteristics of the central sodium type 80 Wh cell developed for basic research. Details of the cell design are summarized in [2], and constants for calculations are listed in Table 1. The calculated results agree well with the measured, and characteristics of the present results are very similar to those reported by many developers of the sodium–sulphur cell [1]. The following are deduced from Figs 1–3.

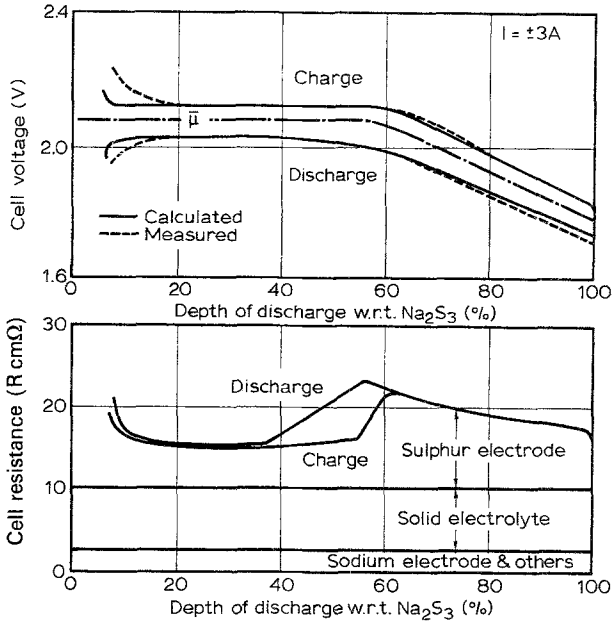

Fig. 1. Charge–discharge characteristics of 80 Wh cell. $I = \pm 3$ A.

(i) If the electric conduction mechanism in the single phase region is common with that in the two phase region, the resistance should decrease gradually in accordance with the depth of discharge, because the ionic resistivity of the melt becomes smaller in accordance with the depth of discharge [6]. On the contrary, the resistance in the single phase region of actual cells is higher than that in the two phase region as shown in Figs 1–3 and in [1, 14, 15]. This seems paradoxical but suggests that the electric conduction in the single

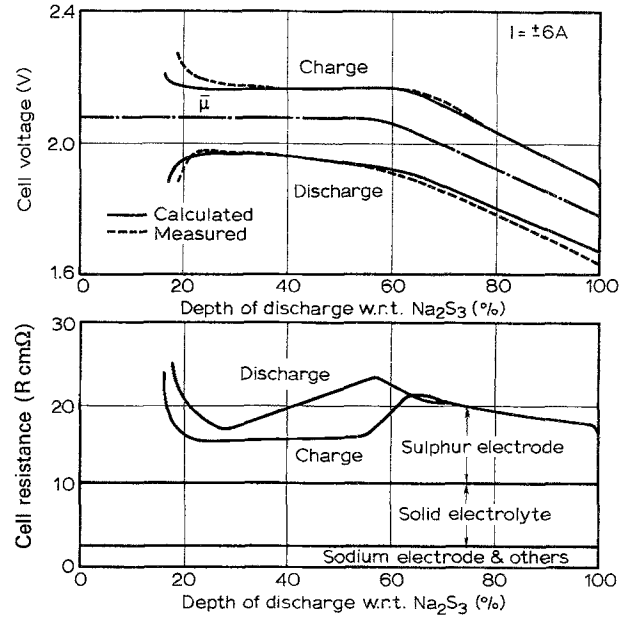

Fig. 2. Charge–discharge characteristics of 80 Wh cell. $I = \pm 6$ A.

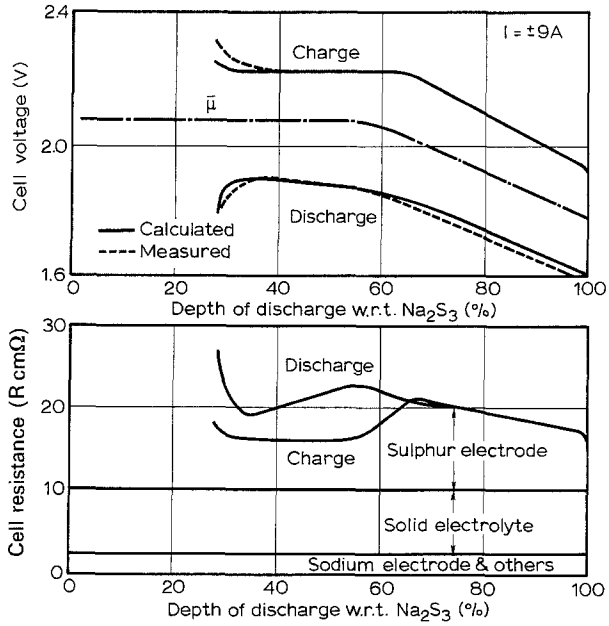

Fig. 3. Charge–discharge characteristics of 80 Wh cell. $I = \pm 9$ A.

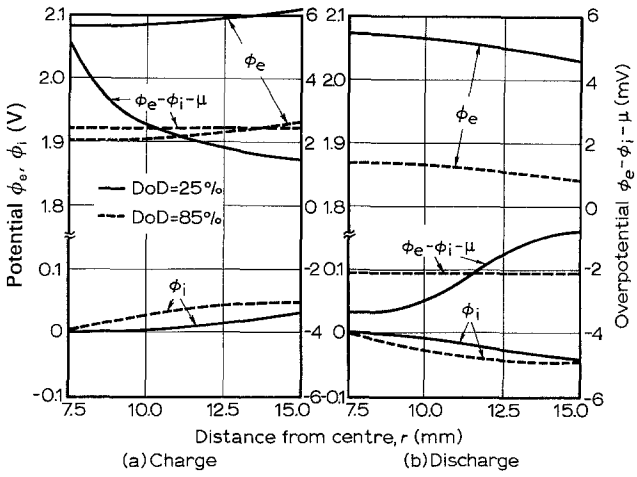

Fig. 4. Distributions of electric potentials and reaction overpotential during charge and discharge operation in the single phase region (25% depth of discharge) and in the two phase region (85% depth of discharge). $I = \pm 6$ A.

phase region is different from that in the two phase region as reported in [9]. That is, the melt composition becomes non-uniform in the single phase region so as to unify the reaction overpotential, and this results in the non-uniform distribution of the electromotive force in the electrode and thus the electrode resistance is increased. Figure 4 shows the distributions of the electric potentials, ϕ_e and ϕ_i, and the reaction overpotential, $\phi_e - \phi_i - \mu$, in the single phase region (85% depth of discharge) and in the two phase region (25% depth of discharge). We can confirm that the reaction overpotential is high at the surface of the solid electrolyte in the two phase region, whereas it is almost uniform in the single phase region.

(ii) On discharge the inflection in the discharge curve occurs at lower depth of discharge than that in the equilibrium OCV curve as the current density increases. On charge, on the other hand, the inflection in the curve occurs earlier at higher current densities. This is also due to the non-uniform concentration distribution during operation. As shown in Fig. 5, even though the averaged composition of the melt remains in the single phase region ($x < 5.24$, depth of discharge > 57%) on charge, the melt composition on the solid electrolyte side partly reaches $Na_2S_{5.24}$ when the charged stage approaches 57% depth of discharge and pseudo-open circuit voltage becomes the constant value, 2.076 V. On the other hand, the molar fraction of sulphur on the electrolyte side becomes smaller than 5.24 on discharge and pseudo-open circuit voltage becomes below 2.076 V, even though the averaged composition still remains in the two phase region.

(iii) The resistance becomes high in the deeply charged stage. This is because the sodium ion concentration at the surface of the solid electrolyte becomes low at the end stage of charge as shown in Fig. 5, i.e. an insulating film of sulphur is formed at the surface of the solid electrolyte and this prevents current passage as reported in [16, 17].

(iv) The calculated voltage in the end stage of charge increases abruptly compared with the measured. This discrepancy may be due to the neglect of axial polarization caused by the axial non-uniformity of the melt porosity in the deeply charged stage [2, 18, 19]. Two-dimensional modelling including capillary effects of the porous sulphur electrode is necessary to perform more accurate simulation at this stage [20].

3.2. *Effect of diffusion*

Figure 6 shows the effect of diffusion. It is recognized that the electric conduction in the single phase region is determined only by the migration. Diffusion due to the concentration gradient is negligible in this region, because the ionic flux due to the potential gradient

Table 1. Constants used for calculations

Item	*Symbol*	*Unit*	*Value*	*Reference*
Weight of initially charged sulphur	W_s	g	100	[2]
Inner radius of sulphur electrode	r_i	cm	0.75	[2]
Outer radius of sulphur electrode	r_o	cm	1.5	[2]
Longitudinal length of sulphur electrode	L	cm	18.0	[2]
Conductivity of graphite matrix	σ_e	$S\,cm^{-1}$	0.5	[10]
Surface area per unit volume of graphite matrix	a_{s0}	$cm^2\,cm^{-3}$	100	[11]
Surface polarization resistance coefficient	K_p	$\Omega\,cm^2$	1.0	[12, 13]

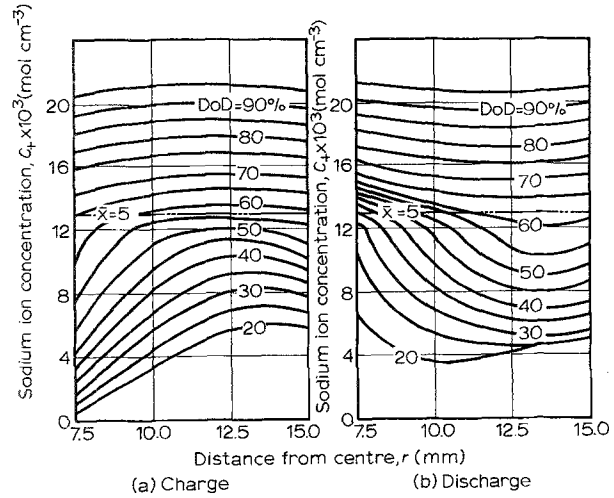

Fig. 5. Distributions of sodium ion concentration during charge and discharge operations. $I = \pm 6$ A.

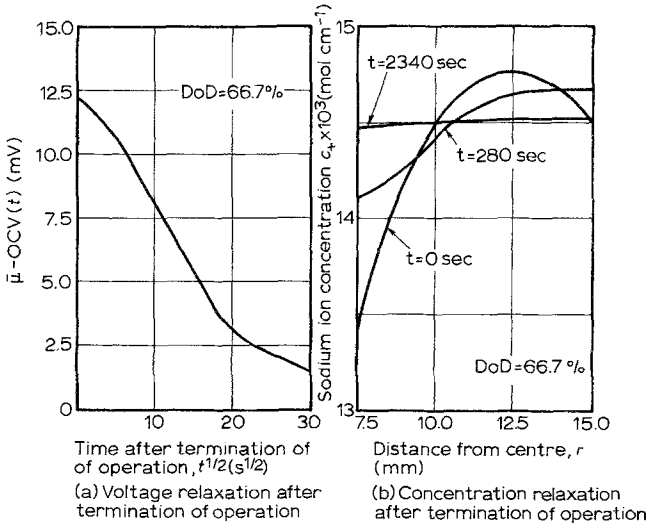

Fig. 7. Transient open circuit voltage and distributions of sodium ion concentration after termination of 6 A charge operation at 66.7% depth of discharge.

is much larger than that due to the concentration gradient. However, since the potential gradient is zero in the two phase region, diffusion performs an important role. If no diffusion exists in the two phase region, the concentration of the sodium ion rapidly becomes low, i.e. the insulating film of sulphur is formed at the surface of the solid electrolyte where the reaction overpotential is high, as shown in Fig. 5. However, it is evident that actual cells are able to be charged up to 80–90% depth of charge [1]. This means the sodium ion concentration at the surface of the solid electrolyte is relaxed by diffusion in the two phase region and high charge acceptance is realized.

3.3. *Quasi-open circuit voltage observed after termination of operation*

Figure 7 shows an example of voltage relaxation and concentration relaxation after termination of 6 A charge in the single phase region. The calculated features are similar to the [9, 15, 21–23]. The following may be concluded.

(i) Since the distribution of the sodium ion concentration is non-uniform in the electrode, the potential gradient exists in the single phase region. Therefore, the open circuit voltage observed after termination of operation in the single phase region is not equal to the equilibrium value but lower after discharge and higher after charge.

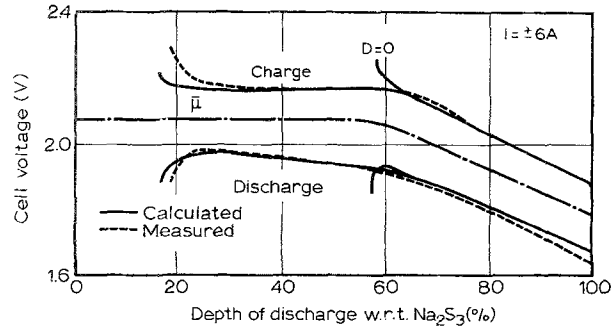

Fig. 6. Charge–discharge characteristics with and without diffusion. $I = \pm 6$ A.

(ii) The transient open circuit voltage gradually approaches equilibrium with a time constant of several minutes in accordance with the concentration relaxation. The voltage is quickly relaxed proportionally to a root of time at an early stage after termination of operation and then the voltage relaxation becomes relatively slow.

4. Conclusions

The dynamic behavior of the porous sulphur electrode of the sodium–sulphur cell is quantified by the present model including diffusion of the reactant. In conclusion, the electric conduction mechanism of the electrode is summarized as follows.

4.1. *In the two phase region*

Sodium ion concentration on the solid electrolyte side becomes low in accordance with the progress of charge and at the final stage of charge the insulating film of sulphur, which restricts the charge acceptance, is formed at the surface of the solid electrolyte. Axial non-uniformity of the melt porosity may accelerate the polarization. Diffusion of the melt relaxes the non-uniformity of the concentration. High charge acceptance is realized by this effect.

On charge the sodium ion flows out of the solid electrolyte and the sulphur mole fraction on the solid electrolyte side becomes smaller than that in the bulk. Therefore, no difficulty exists during discharge. However, since the sulphur mole fraction at the solid electrolyte side becomes less than 5.24, even though the average remains larger than 5.24, the effective resistance becomes gradually higher in accordance with the progress of discharge.

4.2. *In the single phase region*

The distribution of the melt composition in the single phase region is non-uniform so as to unify the distri-

bution of the reaction overpotential. The molar fraction of sulphur is large at the solid electrolyte and metal container side during charge, on the other hand, it is small at these sides during discharge. This non-uniformity results in a quasi-open circuit voltage which is lower during discharge and higher during charge than the equilibrium and thus results in the increase of the effective resistance. The effect of diffusion is negligible in the single phase region, because the ionic flux due to the potential gradient is much larger than that due to the sodium ion concentration.

4.3. *After termination of operation*

The open circuit voltage observed after termination of discharge operation in the single phase region is lower than the equilibrium value and higher after charge due to the non-uniform concentration distribution of the melt composition. It approaches the equilibrium in accordance with concentration relaxation.

Acknowledgement

The author would like to express his appreciation to Y. Kusakabe, H. Hatoh and H. Ajima for their help with the experiments. This work was supported by The Tokyo Electric Power Co., Inc.

References

[1] J. L. Sudworth and A. R. Tilley (eds), 'The Sodium-Sulphur Battery', Chapman and Hall, London (1985).
[2] H. Kawamoto, *J. Electrochem. Soc.* **136** (1989) 1851.
[3] J. Newman, 'Electrochemical Systems', Prentice-Hall, Englewood Cliffs NJ (1973).
[4] K. D. South, J. L. Sudworth and J. G. Gibson, *J. Electrochem. Soc.* **119** (1972) 554.
[5] B. Cleaver and A. J. Davies, *Electrochim. Acta* **18** (1973) 733.
[6] B. Cleaver, A. J. Davies and M. D. Hames, *ibid.* **18** (1973) 719.
[7] S. D. Thompson and J. Newman, *J. Electrochem. Soc.* **136** (1989) 3362.
[8] T. Risch and J. Newman, *ibid.* **135** (1988) 1715.
[9] H. Kawamoto, *Denki Kagaku* **58** (1990) 49.
[10] H. Kawamoto and H. Hatoh, *ibid.* **53** (1985) 366.
[11] Y. K. Kao and P. C. Wayner, Jr., *J. Electrochem. Soc.* **123** (1976) 230.
[12] H. Kawamoto and M. Wada, *ibid.* **134** (1987) 280.
[13] M. Wada, *ibid.* **134** (1987) 631.
[14] M. C. H. McKubre, S. I. Smedley and F. L. Tanzella, *ibid.* **136** (1989) 1962.
[15] B. R. Karas, *ibid.* **132** (1985) 1266.
[16] J. G. Gibson, *J. Appl. Electrochem.* **4** (1974) 125.
[17] General Electric Co., *EPRI Report* EM-2579 (1982).
[18] *Idem, ibid.* EM-3453 (1984).
[19] F. M. Stackpool, Proceedings of the Symposium on Sodium-Sulfur Batteries, A. R. Landgrebe, R. D. Weaver and R. K. Sen, Editors, The Electrochemical Society Softbound Proceedings Series, San Diego CA (1987) 183.
[20] S. A. Naftel, *J. Electrochem. Soc.* **135** (1988) 26C.
[21] S. Mennicke, in 'Advances on Battery Materials and Processes', (edited by J. McBreen, D-T. Chin, R. S. Yeo and A. C. C. Tesung). The Electrochemical Society Softbound Proceedings Series, Pennington NJ (1984) 85.
[22] B. R. Karas, *J. Electrochem. Soc.* **132** (1985) 1261.
[23] A. A. Koening, Proc. DOE/EPRI Beta (Sodium-Sulphur) Battery Workshop VI, EPRI Report AP-6012-SR (1988) 30.